SCAMORSA-1: A camber-morphing wind turbine blade with sliding composite skin

Peter L. Bishay [*], Toby McKinney, Garrett Kline, Maria Manzo, Arthur Parian, Derenik Bakhshi, Andrew Langwald, Abraham Ortega, Matthew Gagnon, Gerbert Funes Alfaro

Department of Mechanical Engineering, California State University, Northridge, Northridge, CA 91330, USA

ARTICLE INFO

ABSTRACT

Wind turbines form an increasingly important source of renewable and sustainable energy. Traditional rigid wind turbine blades are unable to control the flow of air over their surfaces, resulting in higher loads and lower aerodynamic efficiency at non-optimal wind speeds and angles of attack. This paper presents the design of SCAMORSA-1 ("Sliding CAmber- MORphing Skin Action"), a camber-morphing turbine blade in a small scale Horizontal Axis Wind Turbine (HAWT) for increased aerodynamic efficiency and improved extreme load alleviation. The blade is linearly tapered and comprises three sections: a conventional rigid section, a morphing section, and a fixed blade tip, all covered by functionally graded composite skin. Measured from the root, the rigid section spans 0%-60% of the total blade length and its profile transitions at 20% from SD7062 thick airfoil to the thinner SD7037 airfoil. The rigid section includes carbon fiber composite spars that resist flap-wise bending. The morphing section occupies the next 30% of the span with SD2030 airfoil profile and can seamlessly change camber angle up to 10°. This section is composed of three hybrid ribs connected via two leading-edge composite spars and a trailing-edge synchronizing rod. Each hybrid rib has a solid leading-edge segment connected to a flexible trailing-edge segment via T-slots. The trailing-edge segment, where morphing occurs, is an enhanced version of the corrugated FishBAC design, with hexagonal honeycomb infill that increases the out-of-plane stiffness and allows for morphing deformation without internal buckling. Two of these hybrid ribs have servomotors housed in the leading-edge segment. These integrated actuators in the hybrid ribs actuate flexible carbon fiber ribbons that run through slits in the trailing-edge segment to morph it. At the trailing-edge portion of the morphing section, the composite skin transitions to a thin flexible layer that can slide over the deforming trailing-edge segment via skin sliders. Computational simulations were performed to quantify the performance gains and ensure safe operation of all components. A proof-of-concept model of SCAMORSA-1's morphing section was manufactured and tested to demonstrate the effectiveness of the design.

Introduction

Wind energy is a leading competitor in the post carbon-reliant future of global power generation with Horizontal Axis Wind Turbines (HAWT) at the helm. As cutting-edge blade technology continues to improve, overall energy extraction efficiency follows suit [1–6]. Current developments in the wind turbine industry indicate a maximum achieved efficiency of 50% while the theoretical ceiling for wind power generation according to the Betz limit is 59.3%, asserting room for improvement in blade design [1–3]. Wind turbine blades are considered rotating wings, hence many advancements in aircraft wing design can be applied to turbine blades, considering the different loads and boundary conditions. The geometric shapes of modern wind turbine blades are more complicated than aircraft wings since they are twisted and can have nonlinear taper profiles. Modern wind turbine blades come in different sizes, with the larger sizes exceeding the length of a whole commercial transport aircraft. Unlike aircraft wings, the airspeed varies tremendously along the span of turbine blades due to rotation. Wind turbine blades also experience more variations in flow speed and direction given the random nature of wind.

The seamless shape-changing capabilities of birds and other living organisms found in nature inspired engineers and aviators throughout history. However, the rigidity of available materials was a limiting factor [7]. Today, new advances in material technologies have led to

development of morphing designs that are both lightweight and aerodynamically superior to yesterday's designs [8]. Wing morphing can be classified into two categories: in-plane and out-of-plane morphing. In-plane morphing changes the geometric shape of the wing without altering the cross-section of the airfoil. Examples include sweep and span morphing wing designs. Out-of-plane morphing causes the airfoil cross-sectional shape to bend or deform. Examples include camber-morphing, twist-morphing, and chord-morphing designs, as well as morphing winglets.

A lot of previously published research on aeronautical morphing structures have focused mostly on camber-morphing and adaptive trailing-edge technology [9,10]. Camber-morphing is a type of out-of-plane morphing that bends the camber line of the airfoil, varying the local lift distribution. It essentially converts a low-lift airfoil shape into that of a higher performance, high-lift airfoil. Trailing-edge discrete surfaces, currently used on conventional aircraft wings, such as ailerons and flaps, induce drag due to the gaps they create on the wing surface. Camber-morphing surfaces, on the other hand, provide a smooth contour with no additional gaps, thus, avoiding this induced drag. Extensive research has been published proposing methods of camber-morphing techniques [11–21]. One contribution by Woods and Friswell in 2012 [11,12] presented the Fish Bone Active Camber (FishBAC) design. Variations of the FishBAC design were presented by Bishay *et al.* [16] as a shape-memory alloy (SMA) actuated tail structure of an Unmanned Aerial Vehicle (UAV), and by Schlup *et al.* [17] and Bishay *et al.* [18] in the camber-morphing tail stabilizers of MataMorph-2 UAV, and the camber-morphing wings and tail stabilizers of MataMorph-3 UAV, respectively. While the previously mentioned research work included actuators to morph the wings, passive morphing wings, which have compliant trailing-edge sections that can deform under the applied aerodynamic loads with no actuators, also showed superior performance to fixed-wing counterparts [19–21].

A prominent challenge of wing-morphing is the skin design [22]. Ideally, a morphing skin is a continuous surface that can adapt to the contour of the morphing body but remain structurally solid and stable to resist aerodynamic loads. This requires the skin to have conflicting structural requirements including a low in-plane stiffness and a high out-of-plane stiffness [23]. Elastic materials that can handle high strain while maintaining a linear elastic profile were thought to be ideal for use in morphing skin surfaces [24]. Thill *et al.* [25] presented an extensive review of various flexible skins and novel material concepts, emphasizing the use of segmented and corrugated structures, reinforced elastomers, and flexible matrix composite tubes. Although elastomer-based stretchable skins have become popular in morphing applications, they are still susceptible to skin fracturing [26,27]. Hence it is crucial to develop non-stretchable, yet morphing, skin designs. An approach taken by Rediniotis *et al.* [28], presented a bio-inspired morphing skin with sliding segmented rigid panels for a hydrofoil, which showed promising results for out-of-plane camber-morphing. The camber-morphing wings and tail stabilizers in MataMorph-3 UAV [18] also included sliders to enable the skin to slide on the deforming trailing-edge sections, avoiding the need for any stretchable skin.

The implementation of "smart blades" into wind turbines is an emerging field of study with proposed contemporary blades utilizing trailing-edge flaps, twist-morphing or camber-morphing designs to modify in-use blade characteristics [29–39]. Lachenal *et al.* [30] designed a zero torsional stiffness twist-morphing blade that can actively alleviate gust loads which reduce the blade's fatigue life. Daynes and Weaver [31] presented a morphing flap design with an anisotropic cellular structure and integrated servomotors. As part of the INNWind.eu project, Ai *et al.* [33] presented a morphing flap device that comprises a light-weight carbon fiber laminate, 3D-printed honeycomb core, and a flexible silicone surface. Haldar *et al.* [34] designed a morphing trailing-edge flap actuated by multistable laminates. Pohl and Riemenschneider [35] designed a flexible trailing-edge device with a central spine and upper and lower fiberglass composites as flexible

elements. Lambie *et al.* [36] introduced the load-dependent passive camber-control concept for alleviating load fluctuations in wind turbine rotor blades to reduce fatigue and increase durability and blade lifetime. Marten *et al.* [37] and Cordes *et al.* [38] introduced the Adaptive Camber Concept, and applied it locally at an adaptive blade section, not on the entire blade. The approach was very effective in alleviating the applied fluctuating loads and generating higher mean lift forces compared to rigid blades. MacPhee and Beyene [39] proved experimentally and computationally that morphing or flexible wind turbine blades outperform rigid ones, especially when experiencing unfavorable loading conditions. Morphing blades could also produce more power than rigid ones at sub-optimal conditions.

This paper introduces the design of a "Sliding Camber-Morphing Skin Action" blade, named "SCAMORSA-1," which is a camber-morphing small scale horizontal axis wind turbine blade designed to improve aerodynamic performance and extreme load alleviation at varying wind speeds and directions. The design features a morphing section that includes three hybrid ribs, supported by two spars, and connected at the trailing-edge via a synchronizing rod that ensures uniform camber-morphing. The trailing-edge segment of each hybrid rib is a new advancement of the FishBAC design [11,16] with hexagonal honeycomb infill that increases the out-of-plane stiffness and eliminates internal buckling problems encountered in previous designs. The unique PCTPE nylon-based 3D-printing material provided the required stiffness for these flexible segments. Two of the hybrid ribs have integrated servomotors that actuate a flexible composite ribbon which runs through the trailing-edge segment to camber-morph it. A fiberglass composite skin covers the whole blade, but transitions from large thickness around the blade root to moderate thickness on most of the blade surface, and to thin surface over the morphing portion of the skin. Sliders moving in slots in the trailing-edge segments allow the skin to slightly slide over the deforming core to maintain a smooth cambered surface upon actuation. This approach enables camber-morphing with a rigid skin that would maintain the desired shape of the airfoil during actuation and contribute in carrying the aerodynamic loads. The rest of the paper is organized as follows: The next section presents an overview of the preliminary design and sizing process. The following section describes all details of the design. Analysis and simulation results are presented in a separate section after that, followed by the manufacturing and testing section. The paper ends with a summary and conclusions in the last section.

Preliminary design and sizing

SCAMORSA-1 blade has a span of $b = 2$ m, categorizing it among the small HAWT blades. However, a parametric design approach was taken to enable scaling it to larger sizes with adequate replacement of some components to match larger-sized blades. Instead of the optimal Betz nonlinear taper profile that can lead to a fine blade tip, a linear taper profile was used due to its simplicity, with a taper ratio of 0.5. The chord at the root of the blade, c_r, was set to 0.48 m (making $c_r/b = 0.24$) and decreases linearly to 0.25 m before being capped at the tip. Camber-morphing is needed only at a portion of the blade close to the blade tip [37,38]. Hence, the blade is composed of three sections: a solid section that includes the hub connector at the root, a morphing section that is capable of camber-morphing its trailing-edge, and a blade tip section. The location of the camber-morphing section along the span of the turbine blade was studied by Wiratama and Maheri [40]. It was found that the best location for placing a flap on a sample wind turbine blade is at about 70% of the blade span measured from the root of the blade. The size of the flap also has significant effect on the amount of enhancement of average generated power.

SCAMORSA-1 blade incorporates the Selig/Donovan (SD) family of airfoils that were designed for low Reynolds numbers experienced in wind turbines. The turbine blade is considered a cantilever structure. Hence, the maximum bending moment occurs at the blade root which

should be structurally reinforced to ensure safe operation. Accordingly, the SD7062 thick airfoil was chosen at the root of the blade and spans only 0%-10% of the blade length, then smoothly transitions to the moderately thick SD7037 airfoil between 10% and 20% for better aerodynamic performance. SD 7037 airfoil eases the transition into the thin lift-generating airfoil close to the blade tip and maintains structural rigidity and adequate aerodynamic performance. This airfoil occupies 20%-50% of the span. The airfoil profile transitions into the primary airfoil SD2030 completely at 60%, and extends up to the blade tip. The SD2030 airfoil was chosen due to its high aerodynamic efficiency at low Reynolds numbers. This airfoil also has a wide 'drag bucket', which means that its minimum drag coefficient spreads over a large area of lift coefficients, sustaining more laminar flow. Turbine blades are susceptible to buckling and large tip deflections at higher wind speeds, possibly causing the tip to bend out-of-plane and subsequently collide with the tower. A quick transition from the thick SD7062 airfoil to the thin SD2030 airfoil might negatively impact the blade's structural rigidity. Hence, the moderately thick SD7037 airfoil was used in the transitioning portion of the blade contributing to the structural support. Modern turbine blades commonly use multiple airfoil profiles along the blade span to satisfy these various design and performance requirements. The selected span length, chord length, and taper ratio enable enough space within the morphing section of the blade to include servomotors for camber-morphing actuation.

The "QBlade" Wind Turbine Design and Simulation open-source software developed by Herman Föttinger Institute of TU Berlin [41] was used during the preliminary design and sizing process. This software integrates the XFOIL/XFLR5 functionality and a nonlinear lifting line

free vortex wake (LLFVW) algorithm. This lifting line method outperforms the unsteady blade element momentum method used in analysis and design of HAWTs. Multiple models were created with various morphing section length and camber angle in order to study the effects of these two design parameters on the blade performance. Fig. 1 shows a sample computational model developed in QBlade to simulate SCAMORSA-1. QBlade enables integrating a flap into any airfoil and specifying the flap length and angle. Forty sections were used in each model, and morphing was introduced as a flap in the morphing sections' airfoils. All simulations were generated at the same free stream wind speed of 12 m/s, and identical angle of attack and rotational frequency. Comparable turbines on the market with a blade radius of 2 m are rated to perform between windspeeds of 2–15 m/s. Standard sea level (SSL) conditions were assumed (air density $\rho_\infty = 1.225$ Kg/m^3, air pressure P_∞ =101.3 kPa, air temperature $T_\infty = 15°$C).

Running a simulation on QBlade generates plots of lift and drag coefficients, c_l and c_d, of any 2D airfoil section versus angle of attack, α. It also generates a plot of power coefficient, C_p, of the whole turbine versus tip speed ratio, λ. This was done for different camber angles (between 1° and 10°) and morphing section lengths, and compared to a baseline model with no camber. The camber angle is the angle between the tangent to the camber line at the trailing-edge and the airfoil's chord line, as shown in Fig. 2 on SD2030 airfoil.

Fig. 3 and Fig. 4 show the effect of camber angle on c_l and c_l / c_d, whereas Fig. 5 and Fig. 6 show the effect of λ on C_p, both defined as

$$\lambda = \frac{\omega R}{v_\infty}; \qquad C_p = \frac{P}{1/2\rho_\infty A v_\infty^3}, \qquad (1)$$
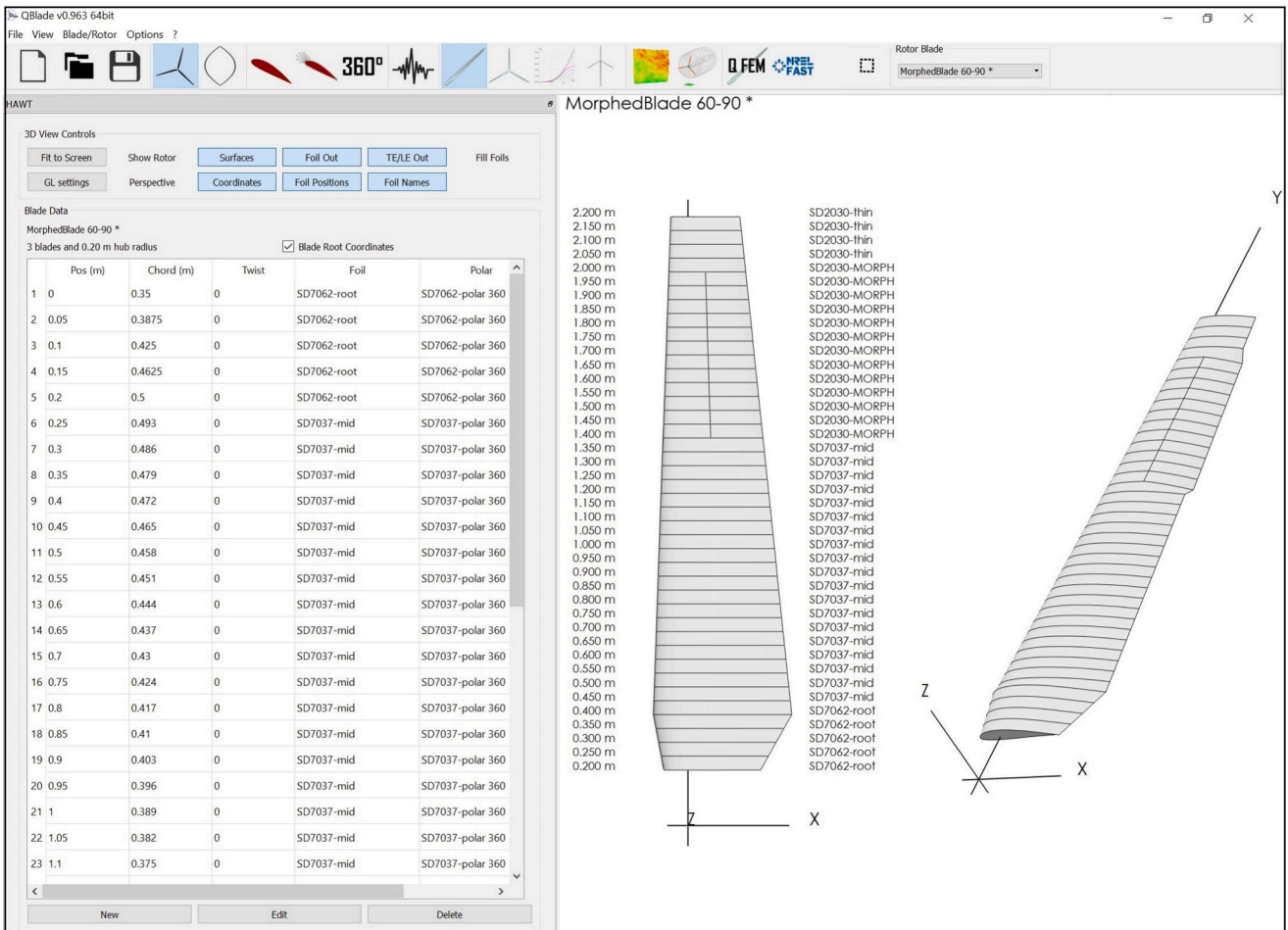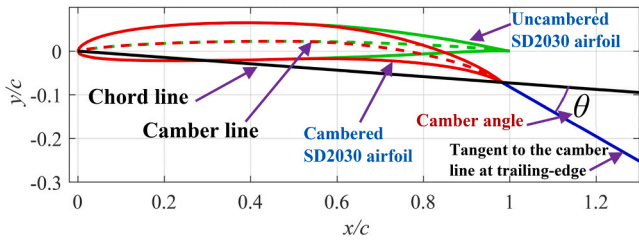

Fig. 1. QBlade model of SCAMORSA-1.

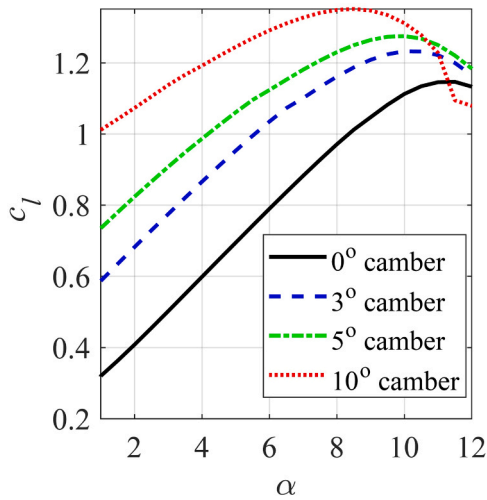**Fig. 2.** Uncambered and cambered SD2030 airfoil and the definition of the camber angle.
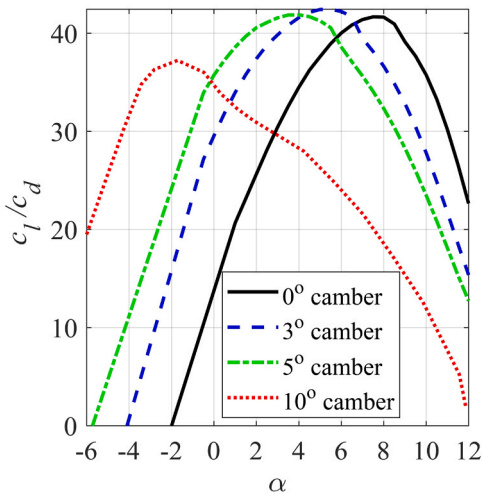

Fig. 3. Effect of camber angle on c_l (SD2030).

Fig. 4. Effect of camber angle on c_l/c_d (SD2030).

where ω is the rotational speed of the rotor in rad/sec, R is the rotor radius, v_∞ is the wind speed at the height of the blade hub, P is the generated power, ρ_∞ is the air density, and A is the turbine frontal area.

The simulation results in Fig. 3 show that as the camber angle increases from 0° to 10°, the maximum value of c_l increases from 1.17 to 1.35, whereas the angle of attack corresponding to this maximum c_l decreases from 11°, for the case of no camber, to 9° for the case of maximum camber angle ($\theta = 10°$).

The results in Fig. 4 show that increasing the camber angle lowers the angle of attack at which maximum aerodynamic efficiency is achieved.
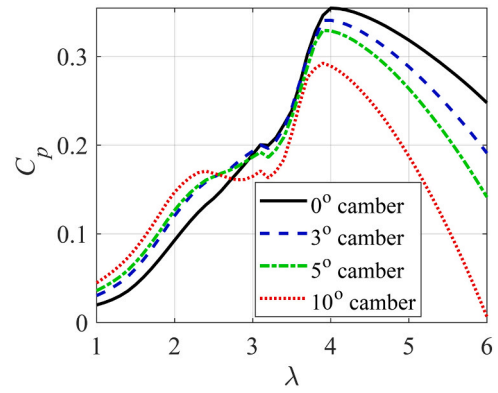

Fig. 5. Effect of λ on C_p at different camber angles with morphing section at 60–90%.
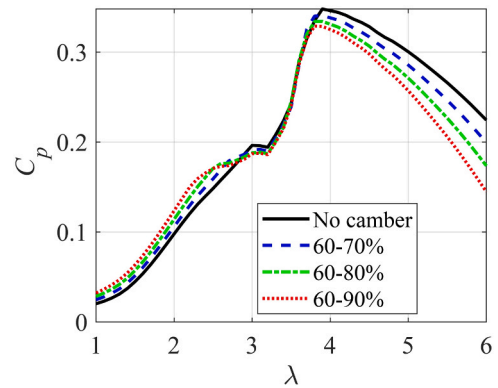

Fig. 6. Effect of λ on C_p at different morphing section locations with 5° camber.

The case of 10° camber angle generates more drag that leads to lower c_l/c_d peak which happens at a negative angle of attack ($\alpha = -2°$). Based on this 2D simulation of SD2030 profile, the 5° camber angle was found to be the best among all considered cases, since it has a high c_l/c_d peak with a relatively wider profile covering a wider range of angles of attack. The ability to control the camber angle via a control system that uses the measured incoming wind direction as an input would lead to the maximum aerodynamic efficiency at varying wind conditions.

Fig. 5 shows the blade's C_p versus λ at various camber angles in the morphing section that extends from 60% to 90% span. It can be seen that at low values of λ, the increase in camber angle leads to higher generated power. As λ approaches 4 and higher, the zero-camber blade generates the highest power coefficient. Again, a camber-morphing blade that is able to control its camber angle according to the measured windspeed would lead to improved performance at a wider range of tip speed ratios. Camber-morphing blades can decrease the cut-in windspeed required to start power generation, compared to traditional blades. Camber-morphing can also increase the cut-out windspeed, or slow the blades down while still generating power, preventing the turbine from shutting down due to excessive rotation. Fig. 6 shows the effect of the morphing section size on the blade's C_p - λ curve, where the camber angle is fixed at 5°. The morphing section in all cases starts at 60% span following the study in [40]. It can be seen that as the morphing section increases in size, C_p increases at low values of tip speed ratios and decreases at high values. Also, longer morphing sections can generate the same amount of power at lower rotational speeds. For example, $C_p = 0.3$ can be achieved with a 60–90% morphing section at 5° camber when $\lambda = 4.5$, while an unmorphed blade would achieve the same power coefficient when $\lambda = 5$. Lower rotational speeds result in lower mechanical stress levels. Simulations with slightly different locations of the morphing section, such as 65%-95%, 70%-80%, 70%-90%, 80%-90%, showed that slight

difference in the blade location has insignificant effect on C_p - λ curve, compared to the size of the morphing section and the camber angle. The location of the morphing section on SCAMORSA-1 was set between 60% and 90%. This makes the chord at the beginning and end of the morphing section, c_{m1} and c_{m2}, to be 0.354 m and 0.279 m, respectively ($c_{m1}/b = 0.177$ and $c_{m2}/b = 0.140$).

Model description

The CAD model of SCAMORSA-1 blade's internal structure is shown in Fig. 7. The blade is entirely covered by a seamless fiberglass composite skin (transparent in the figure to show the internal structure) and houses all internal components. The hub connector is integrated in the rigid section to enable assembling the blade to the wind turbine hub. The rigid section has two carbon fiber composite sandwich spars extending from the hub connection to 55% of the blade length where they are connected to a Balsa wood rib. A flexible foam spacer is placed between the rigid section and the morphing section to enable smooth and seamless transition from the solid airfoil profile in the solid section to the morphing airfoil profile in the morphing section. The surface of the foam is bonded to the composite skin from both sides to ensure smooth transition. The morphing section is composed of three hybrid ribs that are capable of morphing, two of which are active ribs with integrated servomotors. The three ribs are connected via two carbon fiber spars in the leading-edge segments and a synchronizing rod at the trailing-edge segments to ensure uniform camber angle is maintained along the span of the morphing section. The end of the morphing section is connected to another foam spacer and Balsa wood rib, which is connected to the blade tip.

Although the entire blade is covered by a fiberglass composite skin, the thickness of the blade varies spatially to achieve specific design requirements at different locations on the blade. Fig. 8 shows the distribution of composite plies in the composite skin. The root has 5 plies to enhance the structural rigidity of the blade. The rest of the blade section is made up of three plies to balance structural rigidity and low weight. Finally, the skin on the trailing-edge portion of the morphing section is made up of only one ply to provide enough flexibility to deform when camber-morphing actuation is performed in the core. The two strips on both sides of the morphing section (colored yellow in the figure) are the transitional sections between the solid and sliding skins. The core of these two sections is where the flexible foam exists and is covered by a flexible composite skin made of unidirectional fibers in a flexible matrix, similar to the twisting skin presented in [22]. Fiberglass composite laminates possess high specific stiffness and strength, high capacity to withstand corrosion in harsh environments, and low cost. In the following two subsections, more details are provided on the rigid and morphing sections.
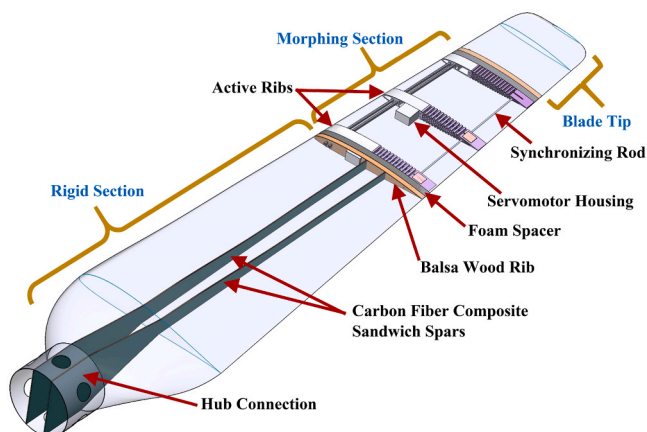

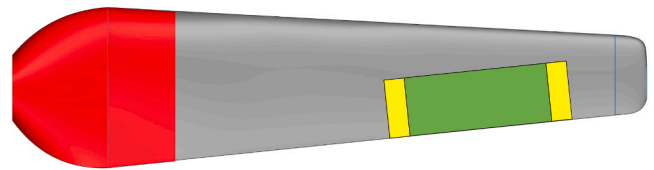
Fig. 7. Internal structure of SCAMORSA-1.

Fig. 8. Distribution of plies in the functionally graded composite skin (red: 5 plies, gray: 3 plies, green: 1 ply, yellow: 1 ply, flexible).

Rigid section design

The two spars that run through the rigid section of the blade are constructed as sandwich composite laminates taking the profile shown in Fig. 9. The structure is composed of two composite face sheets sandwiching a thicker honeycomb core. Each face sheet has three interwoven carbon fiber plies. Sandwich structures provide significantly high bending and buckling stiffnesses and low weight due to the very low density of the core. The spars also provide additional stiffness to the skin. The two spars and the skin form the box structure needed to resist possible torsional loads. The front and rear spars intersect the Balsa wood rib at 45% and 60% of the chord length from the leading-edge, as shown in Fig. 7.

These spars do not go through the morphing section to allow the trailing-edge segments there to deform when camber-morphed. However, leading-edge spars in the morphing section ensure continuous structural rigidity in the farther part of the blade.

Morphing section design

The internal structure of the morphing section is shown in Fig. 10. It spans 60%-90% of the blade and is composed of three hybrid ribs, two carbon fiber leading-edge spars, a synchronizing rod, trailing-edge sliders, and two servomotors in special housings. As mentioned earlier, the thickness of the skin that covers this section decreases as the trailing-edge is approached. Three plies are used above the leading-edge portion and transitions to one ply at the trailing-edge portion that undergoes camber-morphing deformation. The leading-edge spars are made of carbon fiber composite with a square cross section in order to facilitate aligning the ribs precisely. The spars run through the leading-edge segments as well as the foam spacer and Balsa wood rib and are fastened from both sides. Each rib is an assembly of a solid leading-edge segment, 3D-printed of PLA, and a flexible trailing-edge segment, 3D-printed of Plasticized Copolyamide Thermoplastic Elastomer (PCTPE), as shown in Fig. 11. PCTPE is a unique nylon-based 3D-printing material whose stiffness is not as high as Polylactic Acid (PLA) or Acrylonitrile Butadiene Styrene (ABS), but not as low as Thermoplastic polyurethane (TPU). So, it provides the most appropriate stiffness for these components. The design uses a T-joint to connect the two segments as shown in Fig. 11. The airfoil profile in the morphing section is SD2030, but the chord of the ribs decreases as the blade tip is approached, due to the blade taper. To ensure that morphing is uniform spanwise, the length of the trailing-edge segment in the three ribs is constant. However, the change in the chord length is realized in the leading-edge segments that decrease in length as distance increases from the root. Only the first two ribs are considered active ribs with integrated servomotors that actuate
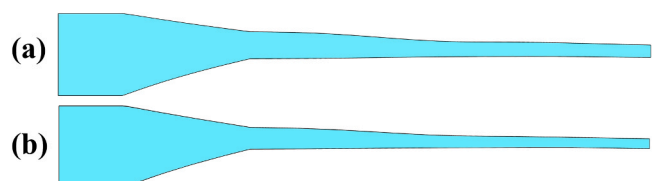
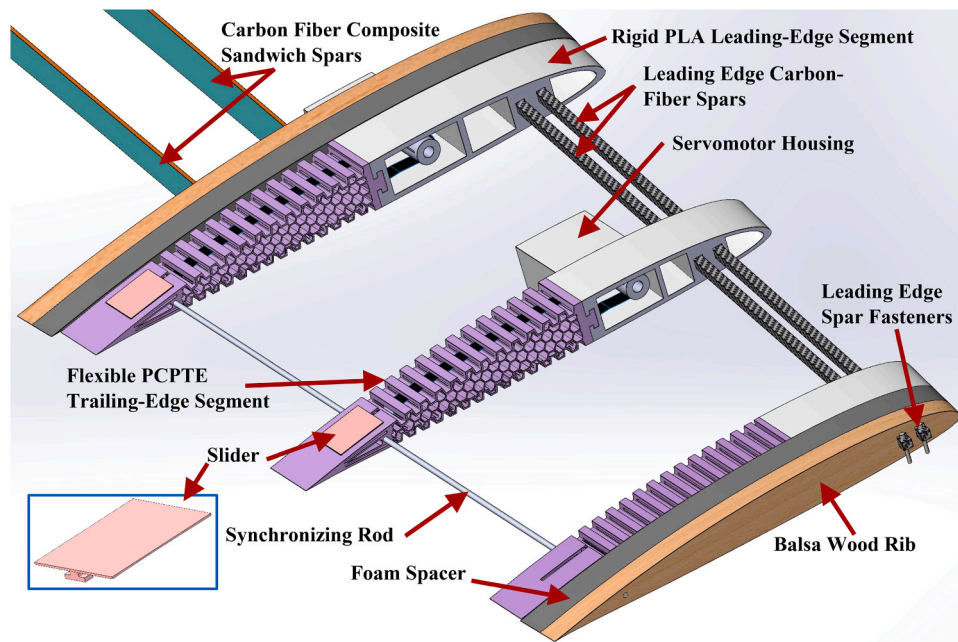

Fig. 9. (a) Front and (b) rear spar profiles.

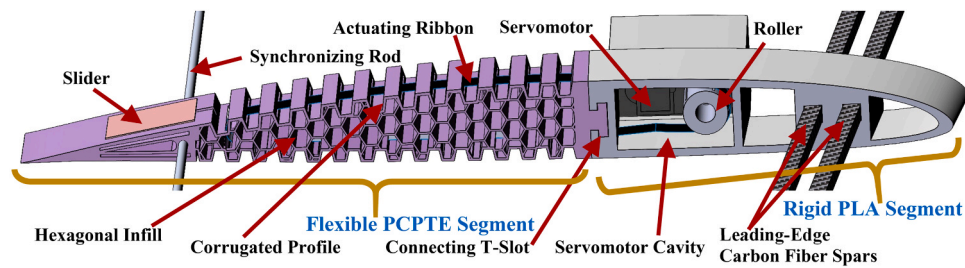**Fig. 10.** Internal structure of the morphing section.

Fig. 11. SCAMORSA-1's active rib.

the trailing-edge segments. The third rib, which is also the smallest, is forced to follow the deformation of the two active ribs via the synchronizing rod.

The outer surface of the trailing-edge segment is corrugated similar to the FishBAC design presented in previous studies [16,18]. However, in order to avoid the internal buckling deformations that happened in the internal structure of many of the previous FishBAC designs, a honeycomb infill is proposed as shown in Fig. 11. The hexagonal shape was selected for this cellular structure according to the recommendations of Heo *et. al.* [42]. This infill increases the out-of-plane stiffness of the rib, preventing it from excessive deformations that can change the airfoil shape at relatively high loads, while maintaining the low bending stiffness needed for camber-morphing with the available actuation forces from the servomotors. Slits are added in the troughs of the corrugated surface to enable a flexible ribbon connected to the servomotor to run through the segment down to the trailing-edge and cause bending actuation. These actuating ribbons are made of a flexible carbon fiber material called Carbitex. The synchronizing rod is made of aluminum with circular cross section and runs through holes in the trailing-edge sections as shown in Fig. 11 to ensure that the three ribs deform uniformly together.

A chordwise slot for the trailing-edge skin sliders is implemented in the trailing-edge segment to allow the sliders that are bonded to the skin to translate during actuation. When camber-morphing occurs, the sliders slide in the slot, moving the skin along with them, as illustrated in Fig. 12. The servomotor housings are placed outside the ribs, but the servomotor shafts are extended in the servomotor cavity of the leading-
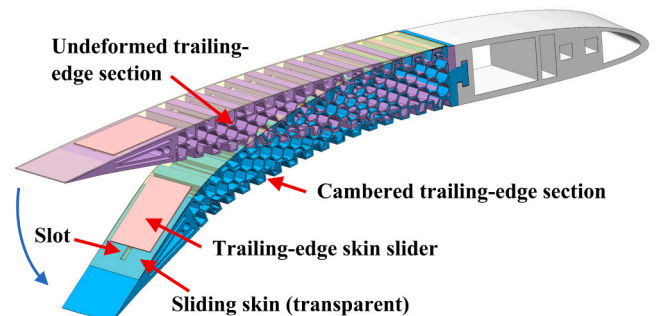

Fig. 12. Illustration of the trailing-edge slider motion (transparent skin).

edge segment. Rollers are mounted to the servomotor shafts and are secured with screws. The Carbitex ribbon is fitted onto these rollers and runs through the slits in the troughs. When the servomotors rotate, the rollers rotate and pull the bottom portion of the Carbitex to morph the section downward.

Analysis and simulation

A static study was performed on the skin alone using 2021 SOLID-WORKS Simulation finite element analysis package, which allows for defining multiple composite laminates on different surfaces in the model. A uniformly distributed pressure load of 160 Pa was applied.

This pressure level was the maximum pressure obtained from a CFD simulation on ANSYS Fluent that considered all input variables mentioned in the preliminary design phase. The uniform distribution was utilized to be on the conservative side. Fixtures were applied at the blade root. The goal of this study was to check if the composite skin alone is stiff enough to withstand the maximum applied loads. A mesh convergence study was performed first by running multiple studies with smaller element sizes or finer meshes. A high-quality standard mesh that includes 541 shell elements (0.079 mm element size) or 1114 nodes was found acceptable with less than 3% error in the maximum displacement. The results showed a maximum displacement of 17.4 mm, and a minimum factor of safety greater than 3%. This study confirmed the adequacy of the skin design to carry the applied loads. The internal structure with its spars and ribs will further stiffen the blade, leading to lower maximum displacement and higher minimum safety factor.

A modal analysis was also performed to ensure that the thin layer of skin at the trailing-edge portion of the morphing section is not introducing a weak point in the blade structure. The first three natural frequencies were found to be 66 Hz, 128 Hz and 344 Hz, and their corresponding vibration modes are shown, respectively, in Fig. 13 (a, b, and c). The first and second modes are bending modes in both directions (transverse and lateral), and the third mode is a twisting mode. The analysis did not find a vibration mode in which the thin skin in the morphing section is vibrating separately within the frequency bandwidth of the study. This ensures that the proposed skin thickness distribution is providing enough support to the skin in the morphing section that prevents it from introducing a structural weak point.

The size of the honeycomb cell in the trailing-edge segment was also studied as shown in Fig. 14. Considering the available torque from the actuating servomotor, it was found that a cell size close to the height of the corrugated troughs would result in the stiffness needed for the desired range of camber angle.

Manufacturing and testing

A proof-of-concept model of the morphing section was manufactured to demonstrate the effectiveness of the proposed design. The solid leading-edge segments and the sliders were 3D-printed of PLA on a Makerbot Replicator+ 3D-printer, whereas the flexible trailing-edge segments were 3D-printed of PCTPE on Ultimaker S5 3D-printer. 3D-printing large parts of nylon-based materials, such as PCTPE, is usually challenging due to bed adhesion problems, despite applying adhesives to the build plate. A simple technique was applied to avoid this problem, where short rectangular pieces were added all around the contour of the model to expand the area of the printed base on the build plate even beyond the limits of the raft. When warping or bed separation happens, it starts from the edges of the printed base and then propagates. So, separation does not reach the area below the model by the end of the print job. After 3D-printing, the two segments of each hybrid rib were assembled first, then the leading-edge composite spars and the synchronizing rod were connected to the ribs, as shown in Fig. 15 (a). The rollers were assembled to the servomotors which were secured in their housings. The waterproof Hexfly 35 Kg servomotor was used in this proof-of-concept model. Carbitex ribbons were fed through the slits of the trailing-edge segments, as shown in Fig. 15 (c), and were then connected to the rollers.

The face sheets of the composite sandwich spars were manufactured first using aluminum mold in an Autoclave, and then another cure cycle was applied to bond the honeycomb core to the face sheets using thin adhesive sheets. Fig. 15 (c) shows the manufactured rear spar. The composite laminated skin would be manufactured using wet layup technique on a coated and polished high-density foam mold that takes the shape of the blade. Different number of plies are added to each portion of the skin as mentioned earlier. For the sake of preliminary testing the proof-of-concept model of the morphing section, and to demonstrate the sliding motion of the trailing-edge skin sliders, a transparent plastic sheet was used as a skin on top of the trailing-edge section. Also, leading-edge sections taking the airfoil profile shape were assembed between the ribs, covering the two leading-edge spars. The assembled proof-of-concept model of the morphing section with the transparent skin is shown in Fig. 16. Fig. 17 (a and b) show the model in an actuation test and confirms the ability of the selected servomotors to achieve a camber-angle even beyond 10°. The test also proved the effectiveness of the skin sliding design. Video V1 in the supplementary material shows the actuation test. It is expected that the stiffness of the final composite skin will be higher than that of the used skin in this test. However, the torque generated by the servomotor is enough to achieve 10° camber.

Supplementary material related to this article can be found online at doi:10.1016/j.jer.2024.04.006.

Summary and conclusion

Wind is a natural phenomenon that is inherently random in its speed and direction at any given location. To extract the maximum amount of energy using a wind turbine without experiencing excessive stress levels, the blades need to be adaptive to the surrounding environment. This work contributes to the ongoing efforts to integrate morphing technology in the wind turbine blade design for improved overall performance at varying conditions. The proposed "SCAMORSA-1" blade design has a camber-morphing section occupying 30% of its span and located closer to the blade tip. The paper presented a preliminary design approach that was guided by a computational model developed in QBlade software package. The hybrid ribs in the morphing sections are the most critical components of this design. The flexible trailing-edge segment of these ribs is an enhanced version of the FishBAC design, with honeycomb infill for improved stability and out-of-plane stiffness. Actuation is produced through servomotors which pull flexible composite ribbons that run through the segment to deform it. Unlike many morphing wing designs in the literature, SCAMORSA-1 does not rely on stretchable skin. One composite skin structure covers the whole blade and is functionally graded by transitioning from thick laminate around the root of the blade, to moderately thick on a large portion of the blade surface. The skin transitions again to a thinner layer that can slide, without stretching, over the morphing core in the morphing section. Computational simulations validated important design decisions. A proof-of-concept model of the morphing section was physically built and tested to validate the design and selected parameters. Future work will focus on building the whole model of the blade and performing different static and dynamic tests. The largest scale that can be achieved with this
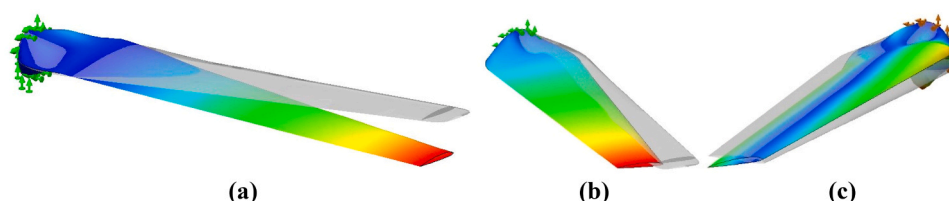

Fig. 13. First three modes of vibration: (a) bending at 66 Hz, (b) lateral bending at 128 Hz, and (c) twisting at 344 Hz.
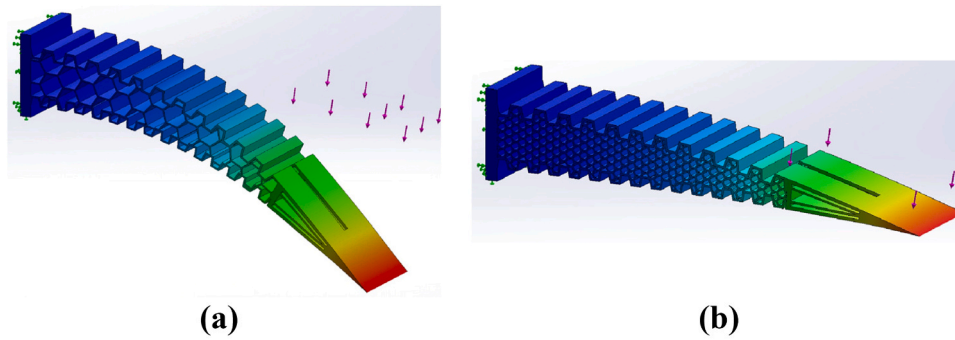
Fig. 14. Deformation of the trailing-edge flexible segment with honeycomb infill of two different sizes: (a) large cell size, (b) small cell size.
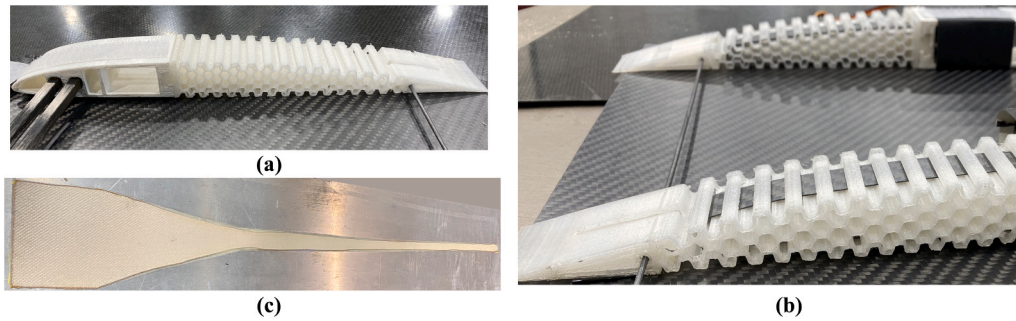

Fig. 15. (a) Assembled rib, (b) Carbitex ribbon inserted, (c) Composite rear spar.
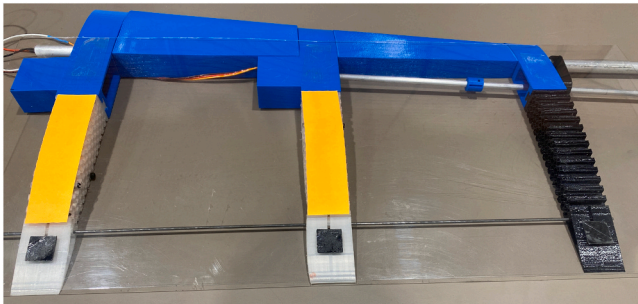

Fig. 16. Assembled proof-of-concept model.

design depends on the manufacturing method that can be used to construct the trailing-edge flexible segments and the availability of actuators for the morphing section. This can also be addressed in future studies.

CRediT authorship contribution statement

Peter L. Bishay: Conceptualization, Data curation, Formal analysis, Funding acquisition, Investigation, Methodology, Project administration, Resources, Software, Supervision, Validation, Visualization, Writing – original draft, Writing – review & editing. **Toby McKinney:** Conceptualization, Data curation, Formal analysis, Investigation, Methodology, Project administration, Software, Validation, Visualization, Writing – original draft. **Garrett Kline:** Conceptualization, Data curation, Formal analysis, Investigation, Methodology, Project administration, Software, Validation, Visualization, Writing – original draft. **Maria Manzo:** Formal analysis, Investigation, Methodology, Software, Visualization, Writing – original draft. **Arthur Parian:** Investigation, Methodology, Software, Writing – original draft. **Derenik Bakhshi:** Investigation, Methodology, Software, Writing – original draft. **Andrew**
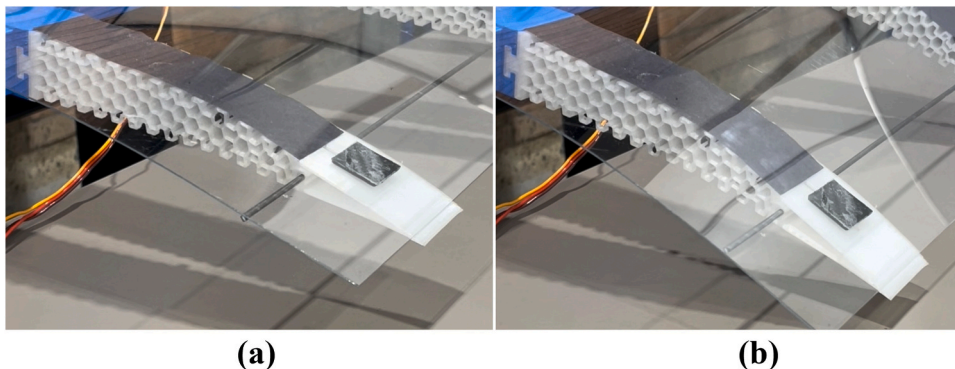

Fig. 17. Preliminary actuation test: (a) undeformed, (b) camber-morphed.

Langwald: Investigation, Methodology, Software, Writing – original draft. **Abraham Ortega:** Investigation, Methodology, Software, Visualization, Writing – original draft. **Matthew Gagnon:** Investigation, Methodology, Software, Writing – original draft. **Gerbert Funes Alfaro:** Investigation, Methodology, Software, Visualization.

Declaration of Competing Interest

The authors declare that they have no known competing financial interests or personal relationships that could have appeared to influence the work reported in this paper.

Acknowledgments

References

[1] U.S. Department of Energy. *Wind vision: A new era for wind power in the United States*. Publication DOE/GO-102015-4557, 1220428. 2015, p. DOE/GO-102015-4557, 1220428.

[2] P.J. Schubel, R.J. Crossley, Wind turbine blade design, Energies Vol. 5 (No. 9) (2012) 3425–3449, https://doi.org/10.3390/en5093425.

[3] B.S. Patil, H.R. Thakare, Computational fluid dynamics analysis of wind turbine blade at various angles of attack and different Reynolds number, Procedia Eng. Vol. 127 (2015) 1363–1369, https://doi.org/10.1016/j.proeng.2015.11.495.

[4] X. Liu, L. Wang, X. Tang, Optimized linearization of chord and twist angle profiles for fixed-pitch fixed-speed wind turbine blades, Renew. Energy Vol. 57 (2013) 111–119, https://doi.org/10.1016/j.renene.2013.01.036.

[5] Ennis, B., Kelley, C., Naughton, B., Norris, R., Das, S., Lee, D., and Miller, D. *Optimized carbon fiber composites in wind turbine blade design*. Publication SAND–2019-14173, 1592956, 682570. 2019, p. SAND–2019-14173, 1592956, 682570.

[6] L. Mishnaevsky, K. Branner, H. Petersen, J. Beauson, M. McGugan, B. Sørensen, Materials for wind turbine blades: An overview, Materials Vol. 10 (No. 11) (2017) 1285, https://doi.org/10.3390/ma10111285.

[7] J. Valasek. Morphing Aerospace Vehicles and Structures, 2nd ed., John Wiley & Sons, Chichester, England, 2012.

[8] Tidwell, Z., Joshi, S., Crossley, W., and Ramakrishnan. S., "Comparison of morphing wing strategies based upon aircraft performance impacts," *45th AIAA/ASME/ASCE/AHS/ASC Structures, Structural Dynamics & Materials Conference,* 2004, Art. 1722. https://doi.org/10.2514/6.2004-1722.

[9] U. Fasel, D. Keidel, L. Baumann, G. Cavolina, M. Eichenhofer, P. Ermanni, Composite additive manufacturing of morphing aerospace structures, Manuf. Lett. Vol. 23 (2020) 85–88, https://doi.org/10.1016/j.mfglet.2019.12.004.

[10] B. Cees, K. Massey, E.J. Abdullah, Wing morphing control with shape memory alloy actuators, J. Intell. Mater. Syst. Struct. Vol. 24 (No. 7) (2013) 879–898, https://doi.org/10.1177%2F1045389×12471866.

[11] B.K.S. Woods, M.I. Friswell, Preliminary investigation of a fishbone active camber concept, Smart Mater., Adapt. Struct. Intell. Syst., Am. Soc. Mech. Eng. Vol. 45103 (Sept. 2012) 555–563, https://doi.org/10.1016/j.ast.2015.01.012.

[12] B.K. Woods, O. Bilgen, M.I. Friswell, Wind tunnel testing of the fish bone active camber morphing concept, J. Intell. Mater. Syst. Struct. Vol. 25 (No. 7) (2014) 772–785, https://doi.org/10.1177/1045389×14521700.

[13] Yokozeki, T., Sugiura, A., and Hirano, Y. Development and wind tunnel test of variable camber morphing wing, *22nd AIAA/ASME/AHS adaptive structures conference,* 2014, Art. 1261. https://doi.org/10.2514/6.2014-1261.

[14] Joo, J.J., Marks, C.R., Zientarski, L. and Culler, A.J., Variable camber compliant wing-design, *23rd AIAA/AHS adaptive structures conference,* 2015, Art. 1050. https://doi.org/10.2514/6.2015-1050.

[15] J. Fincham, M. Friswell, Aerodynamic optimisation of a camber morphing aerofoil, Aerosp. Sci. Technol. Vol. 43 (2015) 245–255, https://doi.org/10.1016/j.ast.2015.02.023.

[16] P.L. Bishay, R. Finden, S. Recinos, C. Alas, E. Lopez, D. Aslanpour, D. Flores, E. Gonzalez, Development of an SMA-based camber morphing UAV tail core design, Smart Mater. Struct. Vol. 28 (No. 7) (2019) 075024, https://doi.org/10.1088/1361-665X/ab1143.

[17] A. Schlup, P.L. Bishay, T. Mclennan, C. Barajas, B. Talbian, G. Thatcher, R. Flores, J. Perez-Norwood, C. Torres, K. Kibret, E. Guzman, MataMorph 2: A new experimental UAV with twist-morphing wings and camber-morphing tail stabilizers, AIAA Scitech 2021 Forum Art. 0584 (2021), https://doi.org/10.2514/6.2021-0584.

[18] Bishay, P.L., Kok, J.S., Ferrusquilla, L.J., Espinoza, B.M., Heness, A., Buendia, A., Zadoorian, S., Lacson, P., Ortiz, J.D., Basilio B., Olvera D. "Design and Analysis of MataMorph-3: A Fully Morphing UAV with Camber-Morphing Wings and Tail Stabilizers Aerospace," Vol. 9, No. 7, 2022, p. 382, https://doi.org/10.3390/aerospace9070382.

[19] K. Taguchi, K. Fukunishi, S. Takazawa, Y. Sunada, T. Imamura, K. Rinoie, T. Yokozeki, Experimental study about the deformation and aerodynamic characteristics of the passive morphing airfoil, Trans. Jpn. Soc. Aeronaut. Space Sci. Vol. 63 (No. 1) (2020) 18–23, https://doi.org/10.2322/tjsass.63.18.

[20] S. Kai, S. Takazawa, S. Ochi, T. Imamura, T. Yokozeki, K. Rinoie, Low-Speed Wind Tunnel Testing of a Passive Camber Morphing Airfoil Using a 3D-Printed Compliant Mechanism. Asia-Pacific International Symposium on Aerospace Technology, Springer Nature Singapore, Singapore, 2021, pp. 1019–1030, https://doi.org/10.1007/978-981-19-2689-1_78.

[21] Ochi, S., Kai, S., Takase, K., Soneda, K., Imamura, T., Rinoie, K., and Yokozeki, T. Aeroelastic Simulation and Experimental Validation of the 3D-printed Passive Morphing Airfoil. In *AIAA SCITECH 2023 Forum* (p. 1766), 2023. https://doi.org/10.2514/6.2023-1766.

[22] P.L. Bishay, C. Aguilar, Parametric Study of a Composite Skin for a Twist-Morphing Wing, , article 259, Aerospace Vol. 8 (No. 9) (2021), https://doi.org/10.3390/aerospace8090259.

[23] V. Ott, D. Keidel, M. Kölbl, P. Ermanni, Investigation of an adaptive, hinge-less, and highly shear stiff structure for morphing skins, J. Intell. Mater. Syst. Struct. Vol. 31 (No. 3) (2020) 445–456, https://doi.org/10.1177%2F1045389×19891527.

[24] Q. Chanzy, A.J. Keane, Analysis and experimental validation of morphing UAV wings, Aeronaut. J. Vol. 122 (No. 1249) (2018) 390–408, https://doi.org/10.1017/aer.2017.130.

[25] C.L. Thill, J. Etches, I. Bond, K. Potter, P. Weaver, Morphing skins, Aeronaut. J. Vol. 112 (No. 1129) (2008) 117–139, https://doi.org/10.1017/S0001924000002062.

[26] D. Ahmad, D. Kumar, R.M. Ajaj, Multiaxial deformations of elastomeric skins for morphing wing applications: theoretical modeling and experimental investigations, Polymers Vol. 14 (No. 22) (2022) 4891, https://doi.org/10.3390/polym14224891.

[27] D. Ahmad, R.M. Ajaj, A Multiaxial Fracture of Ecoflex Skin with Different Shore Hardness for Morphing Wing Application, , 2023, Polymers Vol. 15 (No. 6) (2023) 1526, https://doi.org/10.3390/polym15061526.

[28] O.K. Rediniotis, L.N. Wilson, D.C. Lagoudas, M.M. Khan, Development of a shape-memory-alloy actuated biomimetic hydrofoil, J. Intell. Mater. Syst. Struct. Vol. 13 (No. 1) (2002) 35–49, https://doi.org/10.1177%2F1045389×02013001534.

[29] X. Lachenal, S. Daynes, P.M. Weaver, Review of morphing concepts and materials for wind turbine blade applications: Morphing Concepts and materials for wind turbine blade, Wind Energy Vol. 16 (No. 2) (2013) 283–307, https://doi.org/10.1002/we.531.

[30] X. Lachenal, S. Daynes, P.M. Weaver, A zero torsional stiffness twist morphing blade as a wind turbine load alleviation device, Smart Mater. Struct. Vol. 22 (No. 6) (2013) 065016, https://doi.org/10.1088/0964-1726/22/6/065016.

[31] S. Daynes, P.M. Weaver, A morphing trailing edge device for a wind turbine, J. Intell. Mater. Syst. Struct. Vol. 23 (No. 6) (2012) 691–701, https://doi.org/10.1177/1045389×12438622.

[32] Marten, D., Bartholomay, S., Pechlivanoglou, G., Nayeri, C., Paschereit, C.O., Fischer, A., and Lutz, T. Numerical and experimental investigation of trailing edge flap performance on a model wind turbine. Wind Energy Symposium, Kissimmee, Florida, 2018. https://doi.org/10.2514/6.2018-1246.

[33] Q. Ai, P.M. Weaver, T.K. Barlas, A.S. Olsen, H.A. Madsen, T.L. Andersen, Field testing of morphing flaps on a wind turbine blade using an outdoor rotating rig, Renew. Energy Vol. 133 (2019) 53–65, https://doi.org/10.1016/j.renene.2018.09.092.

[34] A. Haldar, E. Jansen, B. Hofmeister, M. Bruns, R. Rolfes, Analysis of novel morphing trailing edge device actuated by multistable laminates, AIAA J. Vol. 58 (No. 7) (2020) 3149–3158, https://doi.org/10.2514/1.J058870.

[35] Pohl, M., and Riemenschneider, J. Designing and testing a flexible trailing edge for wind energy turbine blades. AIAA/AHS Adaptive Structures Conference, Kissimmee, Florida, 2018. https://doi.org/10.2514/6.2018-1066.

[36] Lambie, B., Jain, M., Tropea, C., and Spelsberg-Korspeter, G. "Passive Camber Change for Wind turbine Load Alleviation." In *49th AIAA aerospace sciences meeting including the new horizons forum and aerospace exposition* (p. 637). https://doi.org/10.2514/6.2011-637.

[37] Marten, D., Spiegelberg, H., Pechlivanoglou, G., Nayeri, C., Paschereit, C.O., & Tropea, C.D. Configuration and numerical investigation of the adaptive camber airfoil as passive load alleviation mechanism for wind turbines. *In 33rd AIAA applied aerodynamics conference* (p. 3390), 2015. https://doi.org/10.2514/6.2015-3390.

[38] U. Cordes, B. Lambie, K. Hufnagel, H. Spiegelberg, G. Kampers, C. Tropea, The Adaptive Camber Concept—A passive approach for gust load alleviation on wind turbines, Wind Energy Vol. 21 (No. 9) (2018) 732–744, https://doi.org/10.1002/we.2190.

[39] D.W. MacPhee, A. Beyene, Performance analysis of a small wind turbine equipped with flexible blades, Renew. Energy Vol. 132 (2019) 497–508, https://doi.org/10.1016/j.renene.2018.08.014.

[40] I.K. Wiratama, A. Maheri, Optimal design of wind turbine blades equipped with flaps, ARPN J. Eng. Appl. Sci. Vol. 9 (No. 9) (2014) 1511–1515, https://doi.org/10.13140/2.1.3075.9689.

[41] Website: ⟨http://www.q-blade.org/⟩. Retrieved on 3/3/2022.

[42] H. Heo, J. Jaehyung, K. Doo-Man, Compliant cellular structures: Application to a passive morphing airfoil (https://doi.org/), Compos. Struct. Vol. 106 (2013) 560–569, https://doi.org/10.1016/j.compstruct.2013.07.013.